PROTEINS
STRUCTURE ■ FUNCTION ■ BIOINFORMATICS

Structural analysis of the N-terminal fragment of the antiangiogenic protein endostatin: A molecular dynamics study

Pedro Henrique Monteiro Torres,[1]* Gabriel Limaverde Soares Costa Sousa,[2] and Pedro Geraldo Pascutti[1]

[1] Instituto de Biofísica Carlos Chagas Filho, Universidade Federal do Rio de Janeiro, Avenida Carlos Chagas Filho 373, 21941-902, Rio de Janeiro, RJ, Brazil

[2] Instituto Nacional de Cancer, Rua André Cavalcanti, 37, 20231-050, Rio de Janeiro, RJ, Brazil

ABSTRACT

Endostatin is a potent antiangiogenic protein derived from the noncollagenous domain 1 (NC1) of collagen XVIII. The mechanism by which endostatin exerts its antiangiogenic effect is still incompletely understood. It has been shown that the 27 amino acid N-terminal fragment of murine endostatin has antitumor, antimigration, and antipermeability activities comparable to the full soluble protein. To understand how this peptide can exert such elaborate function, we performed structural analysis using molecular dynamics to evaluate the behavior of this fragment in aqueous environment. Here, we show that the N-terminal peptide of murine endostatin is able to assume a well-defined structure, folding into a zinc-dependent β-hairpin conformation. Analyzing the folding mechanism, we were able to understand why the N-terminal peptide of human endostatin with the same length failed to acquire a stable conformation. Conversely, we were able to predict the successful folding of the R4Q mutant and of a shorter form of the human peptide with 25 residues. Finally, we show that the β-hairpin conformation assumed by the zinc-bound peptide of murine endostatin has a high structural similarity with fragments of another family of angiogenesis inhibitors: the integrin-binding portion of the NC1 domain of collagen IV. Indeed, our docking simulations show that arresten, canstatin, and the endostatin peptide bind to the same spot of $\alpha V\beta 3$ integrin, suggesting similar interactions via a common binding site on this receptor.

Proteins 2011; 00:000–000.

Key words: endostatin; molecular dynamics; angiogenesis; peptide structure; cancer.

INTRODUCTION

The generation of new blood vessels, a process called angiogenesis, is a fundamental key step in the development of the body but is also pathologically active in several diseases including cancer.[1] Therefore, in the last two decades, some groups have identified new antiangiogenic molecules, among which is endostatin, a 20 KDa globular protein derived from collagen XVIII that was first described in 1997. This first approach has shown that an insoluble *E. coli*-expressed endostatin preparation could inhibit tumor growth and even promote tumor regression showing no significant side effects.[2]

Endostatin is highly conserved in different species, showing 87% of identity between human and mouse sequences.[3] Moreover, some groups reported that human endostatin successfully inhibited tumor growth in murine models, suggesting a well-conserved structural and functional correlation.

Although being one of the most studied endogenous antiangiogenic factors, the mechanism of action of endostatin is still not completely known. Since the endostatin preparations successfully used in the first experiments were obtained and injected as an insoluble aggregate, possibly released as degradation fragments, a common strategy that has been used by several groups is to focus on biologically active endostatin-derived peptides.[4–7]

In 2005, Javaherian and coworkers showed that the N-terminal fragment containing 27 and 25 residues from mouse and human endostatin, respectively, exhibited antitumoral activity analogous to the full-length endostatin. This peptide successfully inhibited tumor growth, VEGF-induced endothelial cell migration, and VEGF-induced vascular permeability in mice bearing Lewis Lung Carcinoma.[8] Further studies showed that the administration of this peptide ameliorated symptoms of several angiogenesis-dependant disorders.[9,10]

Additional Supporting Information may be found in the online version of this article.

*Correspondence to: Pedro Henrique Monteiro Torres, Instituto de Biofísica Carlos Chagas Filho, Universidade Federal do Rio de Janeiro, Avenida Carlos Chagas Filho 373, 21941-902, Rio de Janeiro, RJ, Brazil. E-mail: monteirotorres@biof.ufrj.br

Received 8 February 2011; Revised 2 May 2011; Accepted 13 May 2011
Published online 2 June 2011 in Wiley Online Library (wileyonlinelibrary.com).
DOI: 10.1002/prot.23096

The endostatin N-terminal fragment has three of the four residues responsible for the coordination of a zinc ion on the parent molecule (His1, His3, and His11). The metal was found to be crucial for the antiangiogenic activity of the peptide[8] but its importance on the full-length endostatin molecule is still a matter of debate.[11–13]

On the premise that structure and function are strictly correlated, in this work, we performed molecular dynamics simulations in the microsecond scale to study the dynamics of the N-terminal fragment of endostatin in solution with the aim of characterize structural key elements that may affect its stability. Our simulations show that the endostatin N-terminal peptide clearly folds into a zinc-dependent β-hairpin similar to the integrin-binding domain of other known antiangiogenic proteins. Our findings in this article add some new clues on the mechanism of action of this endostatin-derived peptide.

MATERIALS AND METHODS

To compare the dynamics of the N-terminal of murine and human endostatin, we built the systems depicted on Table I. The crystallographic structures 1BNL[14] and 1DY1,[15] from the RCSB Protein Data Bank[16] were used as templates for the peptides of human and murine endostatin, respectively. We evaluated the influence of the zinc ion (systems 1–4) and of two arginine residues on peptide stability of the human endostatin N-terminal fragment (systems 5 and 6).

Visualization and molecular modeling were made with PyMol[17] and molecular dynamics simulations and analysis were carried out using GROMACS 4.04 software package.[18]

Systems were simulated under NPT ensemble, using GROMOS96 43a1 force field with a time step of 2 fs. The LINCS algorithm was used to constrain all-bonds. Temperature and pressure coupling were done using Berendsen algorithm with reference values of 310K (37°C) and 1 bar, respectively. The PME algorithm was used to treat long-range electrostatics and both van der Walls and Coulomb cut offs were set to 1 nm.

Each peptide was centered in a dodecahedric box filled with explicit SPC water model and the net charge was neutralized with the addition of chloride ions. The zinc ion was described as a divalent cation by the GROMOS96 43a1 force field, it was kept at the same position of the crystallographic structure and no distance restraints were applied. Thus, the zinc coordination was maintained by pure electrostatics interactions as imposed by the force field parameters itself, without the use of artificial restraints. The solvated peptides were then submitted to a sequential energy minimization protocol, consisting of (i) 10,000 steps of steepest descent with position restraints; (ii) 10,000 steps of steepest descent with no restraints, and (iii) 5000 steps of conjugate gradient.

Table I
Amino Acid Sequences of the Peptides Simulated in Each System

System name	Sequence	Ion
H27-Zn	HSHRDFQPVLHLVALNAPLSGGMRGIR	Zn^{++}
H27	HSHRDFQPVLHLVALNAPLSGGMRGIR	N/A
M27-Zn	HTHQDFQPVLHLVALNTPLSGGMRGIR	Zn^{++}
M27	HTHQDFQPVLHLVALNTPLSGGMRGIR	N/A
H25-Zn	HSHRDFQPVLHLVALNAPLSGGMRG	Zn^{++}
H27/R4Q-Zn	HSHQDFQPVLHLVALNAPLSGGMRGIR	Zn^{++}

Due to the fact that the initial conformation based on the crystallographic structure is almost completely extended, all peptides underwent significant changes that were correlated with the folding process on the first nanoseconds of molecular dynamics. Thus, the equilibration phase was included for analysis along with production molecular dynamics.

The RMSD and RMSF values were calculated over the backbone structure. The fluctuation of the terminals was calculated by performing a simple average of the first and last three residues RMSF values. The gromos method was used for generation of conformation clusters, with a cut off of 0.3 nm. Second structure analysis were done using DSSP[19] and the electrostatic potential surfaces were generated using Adaptive Poisson-Boltzmann Solver (APBS).[20]

Molecular docking assays were carried out with the web-based server ClusPro 2.0.[21–24] The crystal structure of $\alpha_v\beta_3$ integrin (PDB id 3IJE[25]) was used as receptor for arresten, canstatin (PDB id 1LI1[26]—A and C chains, respectively) or the M27 peptide with and without the zinc ion. The Supporting Information Videos were rendered using the Visual Molecular Dynamics Software (VMD).[27]

RESULTS

The 27 amino acid peptides of murine and human endostatins exhibit different behavior in solution. Based on the RMS deviation [Fig. 1(A)], cluster analysis [Fig. 1(B,C)], and on the secondary structure data [Fig. 1(D,E)], one can observe that the behavior of the zinc-bound murine (M27-Zn) and human (H27-Zn) peptides are quite distinct. A noteworthy difference is the far superior tendency of the murine peptide to form β-structures, whereas no significant stable structures were observed for the human fragment.

The 27 amino acid peptide of murine endostatin folds into a β-hairpin configuration. RMSD analysis shows that deviation of M27-Zn from the initial configuration gradually increases in a stepwise manner reaching stabilization around 1 nm after 80 ns (Figure 1A, Supporting Information videos 1 and 2), similarly, at about the same time, the structure of the cluster 1 in Figure 1(B) is reached. The large RMSD is due to the significant differ-

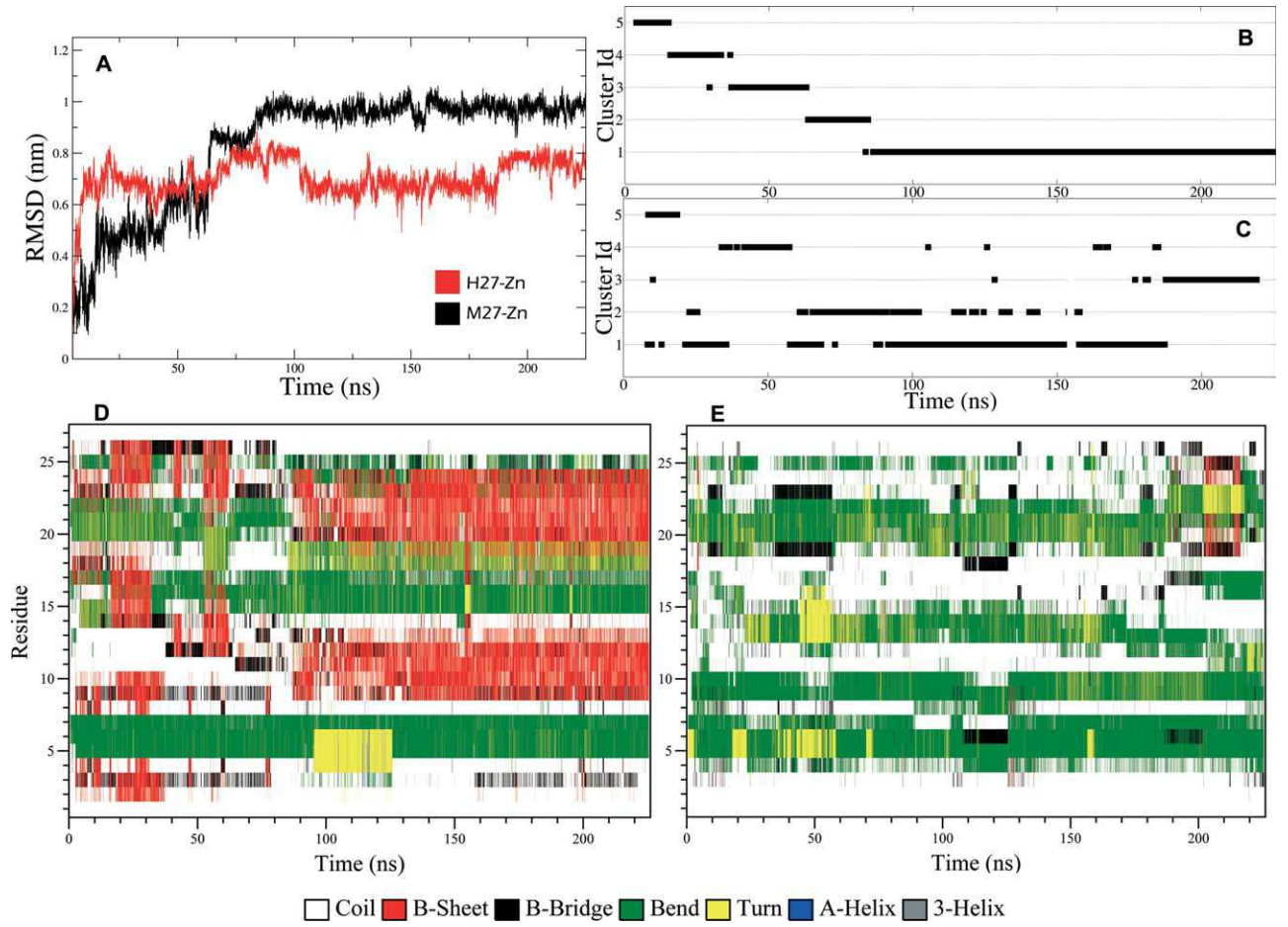

Figure 1

A: RMSD profile of M27-Zn (black) and H27-Zn (red). Although the amino acid sequences are very similar, the dynamics of these peptides are distinct. B: Cluster analysis of M27-Zn. This system presents a cluster progression indicating a gain of stability over time. After ~80 ns, the peptide assumed a stable conformation that lasted until the end of the MD simulation. C: Cluster analysis of H27-Zn. The first cluster (Cluster Id 1) is an intermediate between the several conformations assumed throughout the 225 ns dynamics simulation time. The middle structure of this cluster was used to represent the electrostatic isosurface of H27-Zn in Fig. 2(A). D: Secondary structure analysis of M27-Zn. After ~80 ns, the β-sheet is stabilized and remains stable until the end of the simulation. E: Secondary structure analysis during 225 ns of MD simulation of H27-Zn.

ence between the initial and final conformations. This behavior resembles a folding pathway, with several intermediate states leading to a stable folded conformation, as can be observed in the cluster analysis [Fig. 1(B)].

Conversely, analysis of secondary structure reveals that M27-Zn acquires a hairpin configuration with two stable β-strands after 90 ns [Fig. 1(D)] which remained stable throughout the whole simulation time (225 ns). This main β sheet is formed between the residues 9,10,11,12,13 and 20,21,22,23,24. To further test the stability of this conformation, the molecular dynamics was extended to 1 μs, in which the hairpin remained stable during the whole simulation (Supporting Information Figure 1). On the other hand, H27-Zn structure oscillates and fails to stabilize secondary structures or any stable configuration in 225 ns simulation time [Fig. 1(A,C,E)].

There are only three distinct residues between the murine and human peptide sequences (Table I). The serine (Ser2) and alanine (Ala14) residues in human peptide may cause no relevant conformational difference, but the arginine (Arg4) assigns a positive net charge of +3,0 in contrast with the +2,0 positive net charge of the murine peptide. This extra charge at the N-terminal in H27 peptide may be the main responsible for the conformational destabilization in human peptide, due to the electrostatic repulsion between the N and C-terminal arginines. The presence of the zinc ion increases the positive net charge in both peptides, but it is essential for biological activity, as commented, and its coordination by the three histidine residues (at the positions 1, 3, and 11) confers local stabilization to the chain.

The analysis of electrostatic potential of the 27 amino acid peptide of human endostatin shows a high positive

electrostatic field on both N- and C-terminals [Fig. 2(A)]. The repulsive interaction between these regions explains the instability of this peptide at neutral pH which hence fails to form β-sheets during molecular dynamics. Although Arg4 confers a positive charge to the N-terminal portion of the peptide, it does not affect the zinc ion coordination, since in H27-Zn simulation, the coordination is maintained throughout the whole simulation time (Supporting Information Figure 3A and Supporting Information video 1). This can be explained by the repulsion between the zinc ion and Arg4, which maintains the side chain of this residue away from the ion and prevents steric or eletrostatic disruption of the coordination [Fig. 2(A)]. Javaherian and coworkers used a shorter version of the human peptide (25 instead of 27 residues) which lacks the terminal arginine.[8] Therefore, we tested the effect of the arginines in positions 4 and 27 by building the mutant peptide H27/R4Q-Zn and the peptide H25-Zn, which lacks the terminal arginine (Table I).

RMS fluctuation analysis (RMSF) reveals that the arginine residues on the peptide influence the stability of the terminals. Figure 3(A) shows that H27-Zn, which has one arginine residue at the N-terminal plus two at the C-terminal, has the highest fluctuation on these regions. H25-Zn, with only one arginine residue at each end shows a lower fluctuation at the terminals [Fig. 3(B)] and H27/R4Q-Zn, which has no arginine residues at its N-terminal, displays the lowest values of RMSF of the three systems [Fig. 3(C)]. Secondary structure analysis shows that these two systems in which electrostatic repulsion between terminals were attenuated, have enhanced tendency of forming β-sheets [Fig. 2(B,C)] in comparison with H27-Zn [Fig. 1(E)].

The murine peptide without zinc (M27) displays an abrupt change in RMSD (≈0.25 nm, Supporting Information Figure 2A) oscillating around this value for virtually the entire molecular dynamics simulation. Cluster analysis shows that almost all structures sampled are restricted to a single 0.3 nm-wide RMS cluster (Supporting Information Figure 2B), reaching a stable conformation on the first five nanoseconds of molecular dynamics. Since the peptide was found to be inactive without zinc, we assumed that in the absence of the metal, this peptide collapses into a conformation that has no antiangiogenic activity.

In the initial configuration of all systems where the zinc ion was present, it was coordinated by histidines 1, 3, and 11. The zinc ion coordination was maintained during the whole simulation time on the 27 residue human and murine peptides (H27-Zn and M27-Zn) (Supporting Information Figures 3A and 3C). As mentioned in the materials and methods section, no restraints were applied and the three histidine residues alone were enough to restrict the zinc ion to its site. Moreover, the coordination sphere of the ion was completed by three water molecules in both H27-Zn and M27-Zn systems (see Supporting Information video 1).

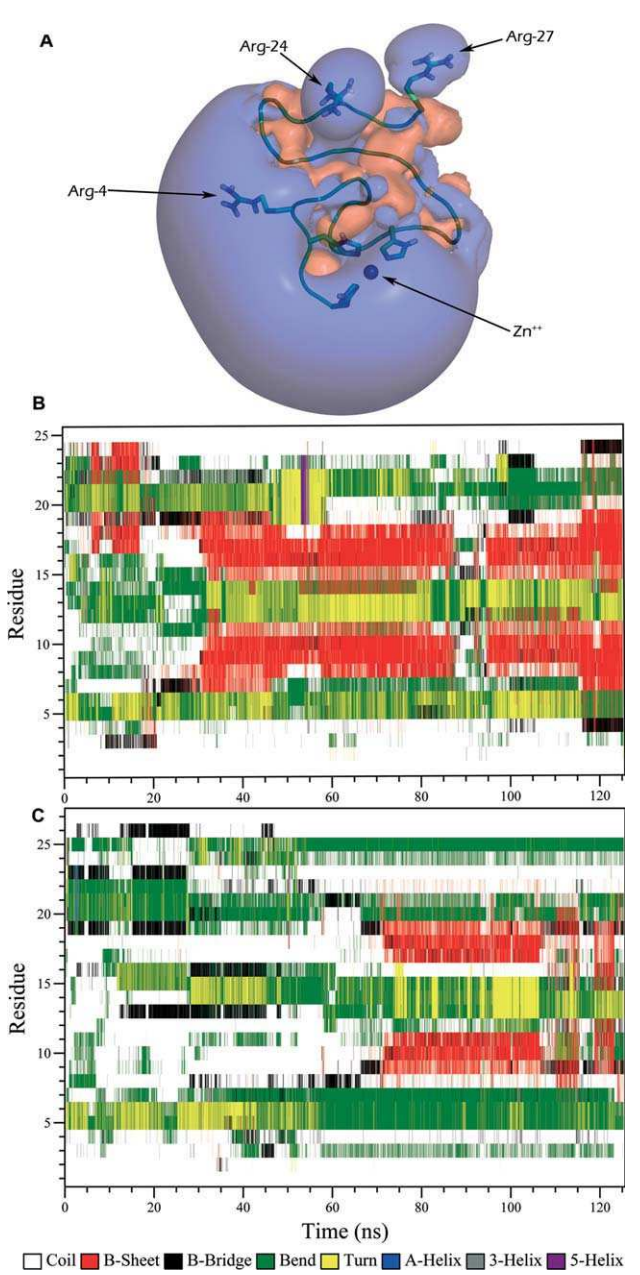

Figure 2

A: Electrostatic potential represented on the isosurface of H27-Zn. The highly positive electrostatic potential near the N-terminal repels the also positively charged arginines near the C-terminal, impairing the stabilization of the structure as a whole. B: Secondary structure analysis of H25-Zn in a 125 ns MD simulation. Unlike H27-Zn, a β-sheet is formed after 20 ns. This phenomenon is associated with the removal of the last arginine residue from the sequence. C: Secondary structure analysis of H25-Zn during 125 ns of MD simulation showing formation of a β-sheet after ~70 ns.

However, the ion coordination was lost during molecular dynamics of the shorter human peptide (H25-Zn) and of the mutated human peptide (H27/R4Q-Zn) (Supporting Information Figures 3E and 3G). The loss of zinc coordination in these systems led to a shift on the position of

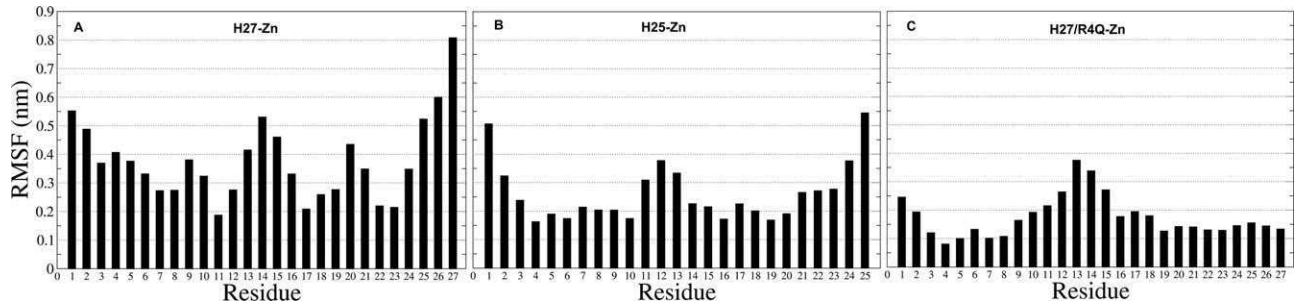

Figure 3

A: RMS fluctuation of H27-Zn from 75 to 125 ns MD simulation time. This time window is the same as the analyzed on Fig. 3(B,C). Note the high values of fluctuation on both terminals. The average fluctuation of the whole peptide is 0.38 nm. B: RMS fluctuation of H25-Zn from 75 to 125 ns MD simulation time. The fluctuation on the terminals is 33.64% lower than H27-Zn. The average fluctuation of the whole peptide is 0.25 nm. C: RMS fluctuation of H27/R4Q-Zn from 75 to 125 ns MD simulation time. The fluctuation on the terminals is 70.32% lower than H27-Zn. The average fluctuation of the whole peptide is 0.14 nm.

the residues in the loop: the amino acids located in the loop on the M27-Zn peptide are Leu15 and Asp16 (Supporting Information Figure 3D), whereas for H25-Zn and H27/R4Q-Zn, the loop is formed by Val13 and Ala14 (Supporting Information Figure 3F and 3H).

These data suggest a very specific role of the zinc ion in the folding of the endostatin N-terminal peptide: initially, the ion must be coordinated by histidines 1, 3, and 11 to induce a correct folding of the peptide into a β-hairpin conformation. Afterward, even upon zinc dissociation, the β-hairpin is maintained, but in a distinct position of the peptide chain. This is verified by the Secondary Structure analysis (Supporting Information Figure 4), where the β-hairpin suffers a shift on its position of three residues when the ion coordination is lost.

After 80 ns simulation time, the M27-Zn peptide assumed a β-hairpin conformation which remained stable throughout the whole simulation time. This main β sheet is formed between the residues 9,10,11,12,13 and 20,21,22,23,24. The system remained on this conformation for ~140 ns. To further test the stability of this conformation, we used it as initial state for a 1 μs MD simulation, in which this structure also remained stable (Supporting Information Figure 1).

The hydrogen-bond analysis of the 1 μs simulation provided us with information about the important bonds for the maintenance of the hairpin structure. All hydrogen bonds that remained stable for at least 20% of the simulation time are detailed in Table II. The most preva-

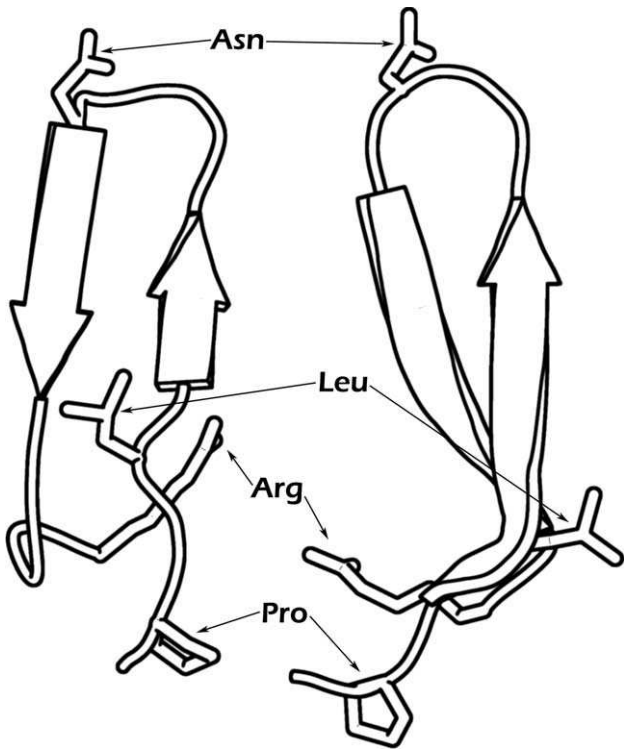

Figure 4

Cartoon and sticks representation of M27-Zn (right) and collagen IV NC1 α1 (arresten) partial crystallographic structure (left). The highlighted residues are in corresponding spatial conformations.

Table II
Most Prevalent Hydrogen Bonds of M27-Zn

Donor	Acceptor	Prevalence (%)
His3 N	Val9 O	84.20
Val9 N	His3 O	73.21
Leu19 N	Leu12 O	72.16
His11 N	His1 O	72.03
Gly21 N	Leu10 O	69.96
Leu12 N	Leu19 O	62.55
Gln7 N	Asp5 O	49.27
Leu10 N	Met23 O	41.35
Ala14 N	Thr17 O	37.88
Gly25 N	Pro8 O	31.15
Leu10 N	Gly22 O	30.93
His11 ND1	Leu19 O	24.53
Arg27 N	Pro8 O	20.67

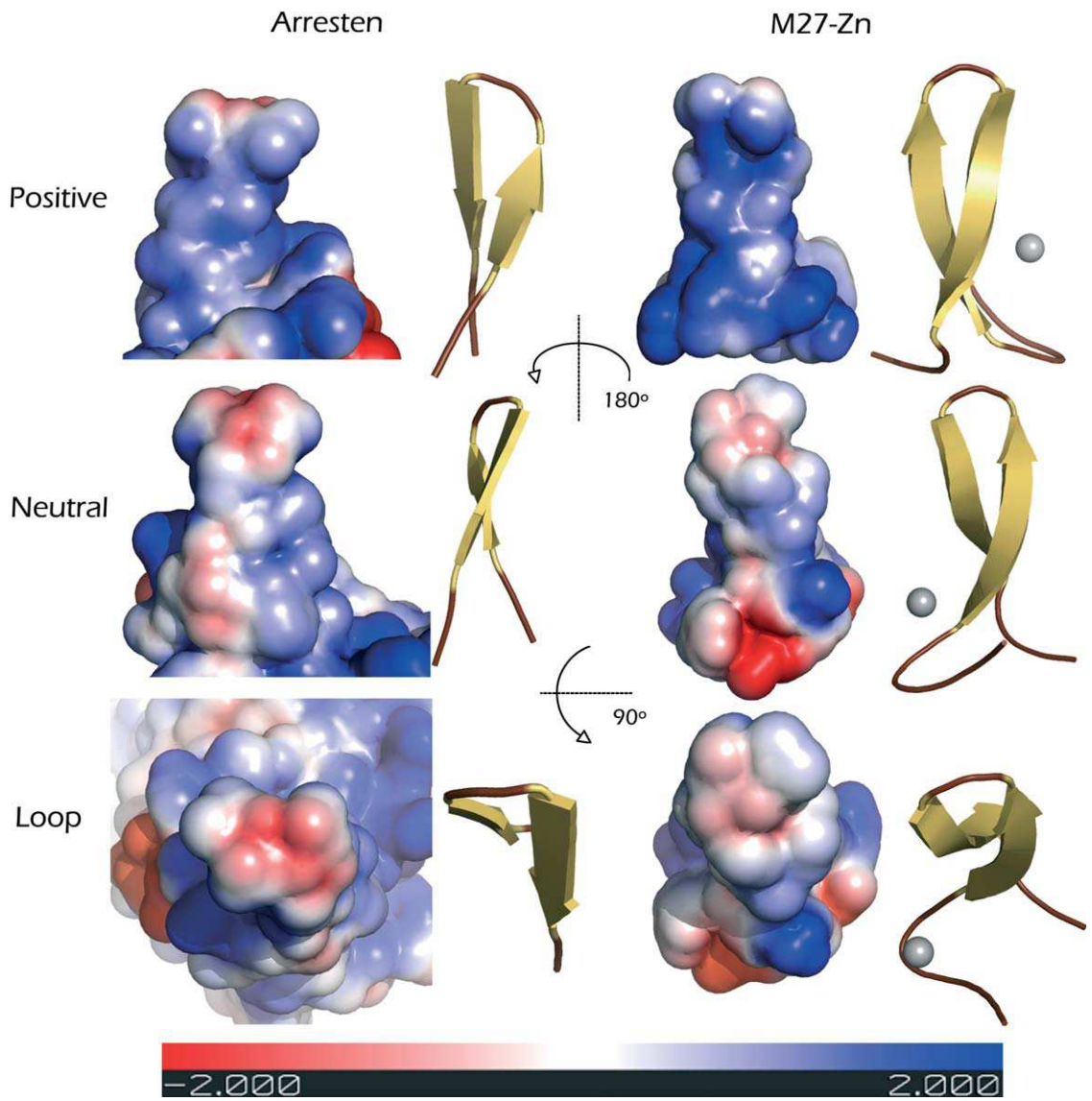

Figure 5

Representation of the electrostatic potential on the solvent accessible surface of arresten (left) and M27-Zn (right). Both present a highly positive domain, a neutral domain and a loop presenting a slightly negative charge. The corresponding cartoon representation and rotation axes are displayed next to the surface representation for better understanding.

lent bonds are formed between residues His3 and Val9, both of which belong to the N-terminal portion of the peptide. These bonds are the main responsible for the stability of the N-terminal bend present in all systems and the N-terminal β-sheet in M27-Zn 1 μs simulation (Supporting Information Figure 1). Other important interactions for the stabilization of this structure are the bonds His11N-His1O and Gln7N-Asp5O along with the zinc coordination.

The most prevalent bonds that form the large β-sheet are formed by residues Leu12 and Leu19. Other important bonds for the stability of this sheet are Leu10N-Met23O, Ala14N-Thr17O, and Leu10N-Gly22O. The bond between Gly25 and Pro8 is the main responsible for the C-terminal stability. The bonds His11ND1-Leu19O and Gly21N-Leu10O are probably involved in the β-hairpin shifting mechanism because their formation requires a small displacement of the residues in the structure.

Since this β-structure exhibited a significant stability, we performed a search for a similar β-hairpin conformation among the structures of known antiangiogenic proteins in the Protein Data Bank. Comparisons were made with antiangiogenic proteins that have a solvent-exposed β-hairpin with approximately the same length of M27-Zn. The search results returned a family of globular pro-

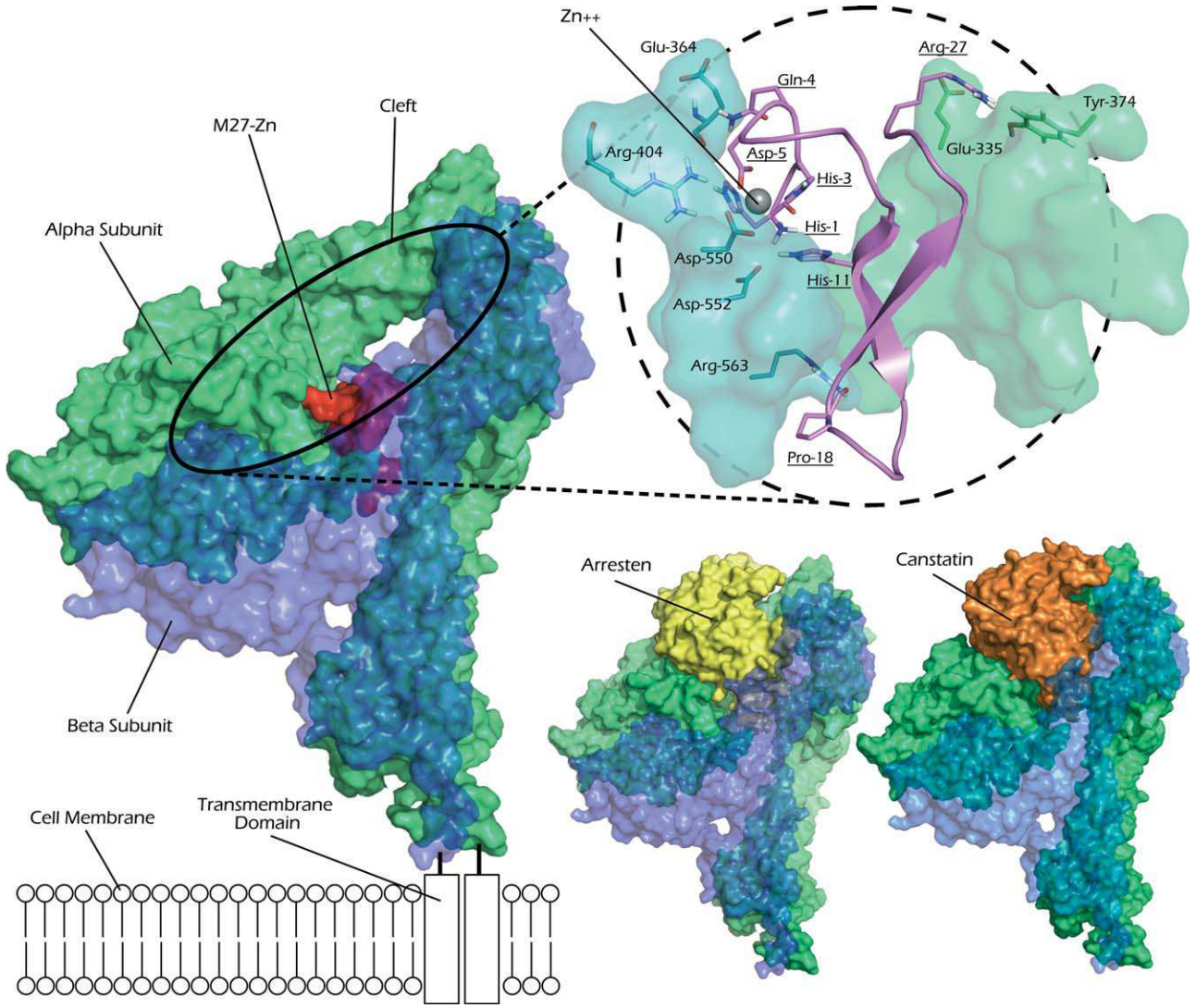

Figure 6

Representation M27-Zn (colored in red at panoramic view and in magenta in detail) docked to αV(green)β3(blue, transparent) integrin (Upper Left). Interaction between the M27-Zn peptide and the integrin in details (Upper Right), the residues showed establish polar contacts (the underlined residues belong to the M27peptide). Docked structures of Arresten (Yellow) and Canstatin (Orange) on integrin αVβ3. Note that all of the ligands bind to the fix domain of the β3 integrin chain and to the head domain of the αV integrin subunit. Also, the much smaller M27-Zn peptide tends to bind deeper in the cleft between the two subunits of the integrin than arresten or canstatin. Docking structures were generated by the web-based server Cluspro 2.0 and displayed with Pymol.

teins derived from collagen IV, specifically the antiangiogenic proteins arresten and canstatin.

Arresten is an endogenous antiangiogenic protein present in the NC1 domain of collagen IV.[28] Its structure displays a prominent β-sheet that resembles the one formed by M27-Zn. Some conserved residues (proline, lysine, asparagine, and arginine) are in spatially correlated positions (Fig. 4).

Another characteristic shared by the β-hairpin of arresten and M27-Zn peptide is the surface electrostatic potential. Both structures exhibit neutral and positively charged moieties. Also, the loop region of these two molecules exhibits a slightly negative potential (Fig. 5).

Although arresten is known to bind $\alpha_1\beta_1$ integrin, its homolog proteins canstatin (Col4A2 NC1) and tumstatin (Col4A3 NC1) both bind to integrin $\alpha_v\beta_3$ and inhibit angiogenesis. Additionally, $\alpha_1\beta_1$ integrin crystallographic structure is not available in the Protein Databank. Thus, we used the crystallographic structure of $\alpha_v\beta_3$ to dock arresten, canstatin, and M27-Zn. We also test if the removal of the zinc ion from the stable M27-Zn β-hairpin structure has influence on the docking results.

The molecular docking results show high tendencies for the zinc-bound M27 peptide (red) and arresten (yellow) to bind $\alpha_v\beta_3$ integrin at the same site: a cleft between the α and β subunits (Fig. 6). The canstatin

Table III
Scores of the Docked Structures Shown in Figure 6

System	Cluster no.	No. of representatives	Score	
M27-Zn	0	152	Center	−958.4
			Lowest energy	−981.0
Arresten	0	51	Center	−992.9
			Lowest energy	−1309.8
Canstatin	5	22	Center	−871.8
			Lowest energy	−922.6

molecule (orange) was also able to interact at the same site, but with smaller probability (Table III) The removal of Zn^{++} from M27 led to interaction in a second binding site, different from the preferred by arresten, indicating that the ion is also important to the site specificity of the peptide (Supporting Information Figure 5).

The M27-Zn peptide conformation in Figure 6 is derived from the representative structure of the most prevalent cluster (Cluster 1). However, the docking algorithm employed by Cluspro 2.0, confers certain flexibility both to the receptor (αVβ3 integrin) and to the ligand (M27-Zn), therefore, the final docked peptide conformation slightly differs from the input structure (0.4 nm α-carbon RMS deviation). As a result, as can be noticed in the docking detail (Fig. 6), an interesting possibility is that Asp5 may also participate in the coordination of the zinc ion creating a tetrahedrical coordination sphere, along with His1, His3, and Asp550 from the integrin β3 subunit.

DISCUSSION

In this work, we studied the dynamics of the N-terminal fragment of endostatin in solution. We described differences in the folding dynamics between the human and murine peptides correlated with minor variations on the primary sequences and analyzed the influence of the zinc ion on the structure of the peptides.

Taken altogether our data suggest that the zinc ion induces a particular β-hairpin folding on the N-terminal fragment of endostatin. Once the hairpin is formed, the structure is maintained even if zinc coordination is lost, but the absence of the metal induces a shift in the β-sheet conformation. Hydrogen bonds analysis indicates that this shift is due to the transient interactions His11ND1-Leu19O and Gly21N-Leu10O. The shift on the β-strand position and the absence of zinc itself may interfere with the binding to a putative receptor.

Arresten[28] is a globular fragment of collagen IV. Another important issue we approached in this work was that the stability of the N-terminal fragment of human endostatin and its ability to form a hairpin configuration are impared by electrostatic repulsion mediated by arginine residues. The peptide stability can be restored by the R4Q mutation or deletion of the C-terminal arginine.

Arresten,[28] canstatin,[29] and tumstatin[30] are angiogenesis inhibitors derived from globular fragments of collagen IV which activity is carried out by a β-hairpin containing structure.[31,32] Considering that endostatin is also a collagen-derived molecule, it is possible that these proteins are functionally related. The similarity between the conformations of M27-Zn and the solvent exposed β-hairpin of these molecules prompted us to perform a docking study of these ligands to a putative common receptor, such as integrin. Although different subtypes are involved, integrin is known to interact with arresten,[33] tumstatin,[30] canstatin,[34] and endostatin.[35] Our results suggest that all these ligands apparently link the mobile domain of the integrin α subunit to the fixed domain of the β subunit. This kind of interaction may impair the mobility of the chains and therefore inhibit integrin activation.

Many authors have studied endostatin fragments and their biological activities (as reviewed by Huanli *et al.*, 2008[36]). These data point to a theoretical multifactorial mechanism of action exerted by several fragments, compatible with the environment in which the antiangiogenic activity of endostatin takes place: the protease-rich extracellular matrix. In this work, we suggest that the N-terminal fragment of endostatin may act through integrin binding after folding into a zinc dependent β-hairpin conformation. These findings will open new perspectives on the development of new endostatin-based drugs.

ACKNOWLEDGMENT

The authors thank CAPES, CNPq and FAPERJ for providing financial support.

REFERENCES

1. Folkman J, Shing Y. Angiogenesis. J Biol Chem 1992;267:10931–10934.
2. O'reilly MS, Boehm T, Shing Y, Fukai N, Vasios G, Lane WS, Flynn E, Birkhead JR, Olsen BR, Folkman J. Endostatin: an endogenous inhibitor of angiogenesis and tumor growth. Cell Press 1997;88:277–285.
3. Oh SP, Kamagata Y, Muragaki Y, Timmons S, Ooshima A, Olsen BR. Isolation and sequencing of cDNAs for proteins with multiple domains of gly-xaa-yaa repeats identify a distinct family of collagenous proteins. Proc Natl Acad Sci USA 1994;91:4229–4233.
4. Cattaneo MG, Pola S, Francescato PE, Chillemi F, Vicentini LM. Human endostatin-derived synthetic peptides possess potent antiangiogenic properties in vitro and in vivo. Exp Cell Res 2003;283:230–236.
5. Francescato P, Chillemi F, Rag E, Cattaneo MG, Pola S, Vicentini L. Studies on the structure-activity relationship of endostatin: synthesis of human endostatin peptides exhibiting potent antiangiogenic activities. J Med Chem 2003;46:4165–4172.
6. Morbidelli L, Donnini S, Chillemi F, Giachetti A, Ziche M. Angiossupressive and angiostimulatory effects exerted by synthetic partial sequences of endostatin. Clin Cancer Res 2003;9:5358–5369.
7. Wickström SA, Alitalo K, Keski-Oja J. An endostatin-derived peptide interacts with integrins and regulates actin cytoskeleton and migrtion of endothelial cells. J Biol Chem 2004;279:20178–20185.

8. Sjin RMTT, Stachi-Fainaro R, Birsner AE, Ramanujam VMS, Folkman J, Javaherian K. A 27-amino-acid synthetic peptide corresponding to the nh_2-terminal zinc-binding domain of endostatin is responsible for its antitumor activity. Cancer Res 2005;65:3656–3653.
9. Becker CM, Sampson DA, Short SM, Javaherian K, Folkman J, D'amato RJ. Short synthetic endostatin peptides inhibit endothelial migration in vitro and endometriosis in a mouse model. Fertil Steril 2006;85:71–77.
10. Tanabe K, Maeshima Y, Ichinose K, Kitayama H, Takazawa Y, Hirokoshi K, Kinomura M, Sugiyama H, Makino H. Endostatin peptide, an inhibitor of angiogenesis, prevents the progression of peritoneal sclerosis in a mouse experimental model. Kidney Int 2005;71:227–238.
11. Boehm T, Folkman J, Browder T, O'Reilly MS. Antiangiogenic therapy of experimental cancer does not induce acquired drug resistance. Nature 1997;390:404–407.
12. Sim BK, Fogler WE, Zhou XH, Liang H Madsen JW, Luu K, O'Reilly MS, Tomaszewski JE, Fortier AH. Zinc ligand-disrupted recombinant human endostatin: potent inhibition of tumor growth, safety and pharmacokinetic profile. Angiogenesis 1999;3:41–51.
13. Yamaguchi N, Anand-Apte B, Lee M, Sasaki T, Fukai N, Shapiro R, Que I, Lowik C, Timpl R, Olsen BR. Endostatin Inhibits VEGF-induced endothelial cell migration and tumor growth independently of zinc binding. EMBO 1999;18:4414–4423.
14. Ding YH, Javaherian K, Lo KM, Chopra R, Boehm T, Lanciotti J, Harris BA, Li Y, Shapiro R, Hohenester E, Timpl R, Folkman J, Wiley DC. Zinc-dependent dimers observed in crystals of human endostatin. Proc Natl Acad Sci USA 1998;95:10443–10448.
15. Hohenester E, Sasaki T, Mann K, Timpl R. Variable zinc coordination in endostatin. J Mol Biol 2000;297:1–6.
16. Berman HM, Westbrook J, Feng Z, Gilliland G, Bhat TN, Weissig H, Shindyalov IN, Bourne PE. The protein data bank. Nucleic Acids Res 2000;28:235–242.
17. Delano WL, The pymol molecular graphics system. San Carlos, CA, USA: Delano Scientific; 2002. Available at:http://www.Pymol.Org.
18. Van Der Spoel D, Lindahl E, Hess B, Groenhof G, Mark AE, Berendsen HJC. Gromacs: fast, flexible and free. J Comp Chem 2005;26:1701–1718.
19. Kabsch W, Sanders C. Dictionary of protein secondary structure: pattern recognition of hydrogen bonded and geometrical features. Biopolymers 1983;22:2577–2637.
20. Baker NA, Sept D, Joseph S, Holst MJ, Mccammon JA. Electrostatics of nanosystems: application to microtubules and the ribosome Proc Natl Acad Sci USA 2001;98:10037–10041.
21. Kozakov D, Hall DR, Beglov D, Brenke R, Comeau SR, Shen Y, Li K, Zheng J, Vakili P, Paschalidis IC, Vajda S. Achieving reliability and high accuracy in automated protein docking: cluspro, piper, sdu, and stability analysis in Capri rounds 13–19. Proteins 2010;78:3124–3130.
22. Kozakov D, Brenke R, Comeau SR, Vajda S. Piper: an fft-based protein docking program with pairwise potentials. Proteins 2006;65:392–406.
23. Comeau SR, Gatchell DW, Vajda S, Camacho CJ. Cluspro: an automated docking and discrimination method for the prediction of protein complexes. Bioinformatics 2004;20:45–50.
24. Comeau SR, Gatchell DW, Vajda S, Camacho CJ. Cluspro: a fully automated algorithm for protein-protein docking. Nucleic Acids Res 2004;32 (Suppl 2):W96–W99.
25. Xiong XP, Mahalingham B, Alonso JL, Borrelli LA, Rui X, Anand S, Hyman BT, Rysiok T, Müller-Pompalla D, Goodman SL, Arnaout MA. Crystal structure of the complete integrin αvβ3 ectodomain plus an α/β transmembrane fragment. J Cell Biol 2009;186:589–600.
26. Than ME, Henrich S, Huber R, Ries A, Mann K, Kühn K, Timpl R, Bourenkov GP, Bartunik HD, Bode W. The 1.9-Å crystal structure of the noncollagenous (nc1) domain of human placenta collagen IV shows stabilization via a novel type of covalent met-lys cross-link. Proc Natl Acad Sci USA 2002;99:6607–6612.
27. Humphrey W, Dalke A, Schulten K. VMD—visual molecular dynamics. J Mol Graph 1996;14:33–38.
28. Colorado PC, Torre A, Kamphaus G, Maeshima Y, Hopfer H, Takahashi K, Volk R, Zamborsky ED, Herman S, Sarkar PK, Ericksen MB, Dhanabal M, Simons M, Post M, Kufe DW, Weichselbaum RR, Sukhatme PV, Kalluri R. Anti-angiogenic cues from vascular basement membrane collagen. Cancer Res 2000;60:2520–2526.
29. Kamphaus GD, Colorado PC, Panka DJ, Hopfer H, Ramchandran R, Torre A, Maeshima Y, Mier JW, Sukhatme VP, Kalluri R. Canstatin, a novel matrix-derived inhibitor of angiogenesis and tumor growth. J Biol Chem 200;275:1209–1215.
30. Maeshima Y, Colorado PC, Torre A, Holthaus KA, Grunkemeyer JA, Ericksen MB, Xiao Y, Stillman IE, Kalluri R. Distinct antitumor properties of a type iv collagen domain derived from basement membrane. J Biol Chem 2000;275:21340–21348.
31. Eikesdal HP, Sugimoto H, Birrane G, Maeshima Y, Cooke VG, Kieran M, Kalluri R. Identification of amino acids essential for the antiangiogenic activity of tumstatin and its use in combination antitumor activity. Proc Natl Acad Sci USA 2008;105:15040–15045.
32. He GA, Luo JX, Zhang TY, Wang FY, Li RF. Canstatin-n fragment inhibits in vitro endothelial cell proliferation and suppresses in vivo tumor growth. BBRC 2003;312:801–805.
33. Nyberg P, Xie L, Sugimoto H, Colorado P, Sund M, Holthaus K, Sudhakar A, Salo T, Kalluri R. Characterization of the antiangiogenic properties of arresten, an α1β1 integrin-dependent collagen-derived tumor suppressor. Exp Cell Res 2008;314:3292–3305.
34. Magnon C, Galaup A, Mullan B, Rouffiac V, Bidart JM, Griscelli F, Opolon P, Perricaudet M. Canstatin acts on endothelial and tumor cells via mitochondrial damage initiated through interaction with αvβ3 and αvβ5 integrins. Cancer Res 2005;65:4353–4361.
35. Faye C, Moreau C, Chautard E, Jetne R, Fukai N, Ruggiero F, Humphries MJ, Olsen BR, Ricard-Blum S. Molecular interplay between endostatin, integrins and heparan sulfate. J Biol Chem 2009;284:22029–22040.
36. Xu HL, Tan HN, Wang FS, Tang W. Research advances of endostatin and its short internal fragments. Curr Prot Pept Sci 2008;9:275–283.